Supplementary information

The effect of separation distance on hydrogen spillover in Os promoted Co@HCS catalysts

Table of Contents

1.1 Catalyst characterization

TEM analysis was performed on a Tecnai spirit (T12) transmission electron microscope operating at 120 kV. The samples were dispersed in methanol by ultra-sonication and loaded onto a copper grid for TEM analysis. The particle size distribution of the materials formed was determined by counting at least 200 randomly selected particles per sample from different TEM images. Gaussian statistics yielded values for the average particle sizes. The bulk crystalline phase composition of the catalysts was studied using a Bruker D2 Phaser powder X-ray diffractometer equipped with a Co−Kα X-ray source (λ = 1.7889 Å), a flat plate sample stage and a Lynxeye PSD detector. The scan range was from 10° to 90° 2θ in 0.0260°.

The thermal stability of the samples was monitored by using a PerkinElmer STA6000 analyser (Fig. 3.7). Each sample (~10 mg) was heated from 50 to 900 °C at a heating rate of 10 °C/min in an oxidizing atmosphere maintained by flowing air (10 mL/min). The thermogravimetric analysis with differential thermal gravimetry (TGA-DTG) profiles were recorded from 10 mg samples without any prior treatment. TGA data provided a plot of the loss in sample weight as various components of the sample decomposed as a function of temperature, whereas DTG results allowed for an easy identification of the maximum temperature where the decomposition took place.

N_2 adsorption−desorption experiments were conducted at −195 °C using a Micromeritics Tristar 3000 surface area and porosity analyser. Prior to an experiment, the sample was outgassed at 150 °C for 4 h under N_2 gas. The BET surface areas were obtained from adsorption data in a relative pressure range from 0.05 to 0.30. The total pore volumes were calculated from the amount of N_2 vapour adsorbed at a relative pressure of 0.99. The pore size distributions were evaluated from the desorption branches of the isotherms using the Barrett−Joyner−Halenda (BJH) method. The micropore surface area and volume were calculated using t-plot data.

TPR experiments were carried out with a Micromeritics Auto Chem II unit. The catalyst (approximately 50 mg) was placed in a tubular quartz reactor, fitted with a thermocouple for continuous temperature measurement. The reactor was heated in a furnace. Prior to the temperature-programmed reduction measurement, the calcined catalysts were flushed with high purity Ar gas at 200 °C for 30 min, to remove water and impurities, followed by cooling to ambient temperature. Then, the gas supply was switched to 5% H_2/Ar, and the temperature was raised at a rate of 10 °C min^{-1} from 50 to 850 °C. The gas flow rate through the reactor was controlled by three Brooks mass flow controllers and was kept constant at 50 $mL.min^{-1}$. The H_2 consumption (TCD signal) was recorded automatically. Pulse chemisorption was performed using the Micromeritics Auto Chem II instrument, to compute the number of active sites on the catalysts. The catalyst (ca. 100 mg) was placed in a tubular quartz reactor. The sample was reduced at 350 °C for 2 h under a H_2 flow of 50 $mL.min^{-1}$. Before injection of the active gas, the sample was purged using helium gas at 350 °C for 1 h, followed by cooling to ambient conditions.

1.2 Data Reduction and Interpretation

For all PXRD data presented, the crystalline phase identification was done using DIFFRAC.EVA (Version 4.2. Release 2016) using the crystallography open database (COD) (Release 2020). Phase analysis was done using the Rietveld method as implemented in Bruker AXS TOPAS software (Version 5, 2014). HCS diameter and carbon shell thickness were determined using TEM images and ImageJ software (1.48 version).

1.3 Fischer-Tropsch Synthesis catalyst evaluation

The FTS reaction was performed in a fixed-bed micro-reactor. A gas cylinder containing a $H_2/CO/N_2$ mixture (~60/30/10 vol %; purity 99.99%) was used to supply the reactant gas stream to the catalyst with a specific space velocity of 1800 mL h^{-1} g^{-1}. N_2 was used as an internal standard in order to ensure accurate mass balances. Catalyst (0.5 g, sieved through a 150 µm mesh, without pelletizing) was added to the reactor (resulting catalyst bed ~4 cm in length) and reduced in situ at 350 °C for 2 h under a stream of H_2 (1.5 bar at 50 mL.min^{-1}). After reduction, the reactor temperature was decreased to ambient temperature under a hydrogen flow and then heated up to 220 °C under synthesis gas at a pressure of 10 bar. A hot trap placed immediately after the reactor was held at 150 °C in order to collect wax. A second trap kept at ambient temperature was used to collect the oil and water mixture. All gas lines after the reactor were kept at 100 °C. The flow was controlled using a metering valve and measured by a bubble meter. The product stream was analysed online using two gas chromatographs. A thermal conductivity detector (TCD), equipped with a Porapak Q (1.50 m × 3 mm) packed column, was used to analyse H_2, N_2, and CO, and a flame ionization detector (FID), equipped with a Porapak Q packed column, was used for the analysis of the hydrocarbons online using the Clarity software package.

List of Figures

1.4 Thermogravimetric analysis

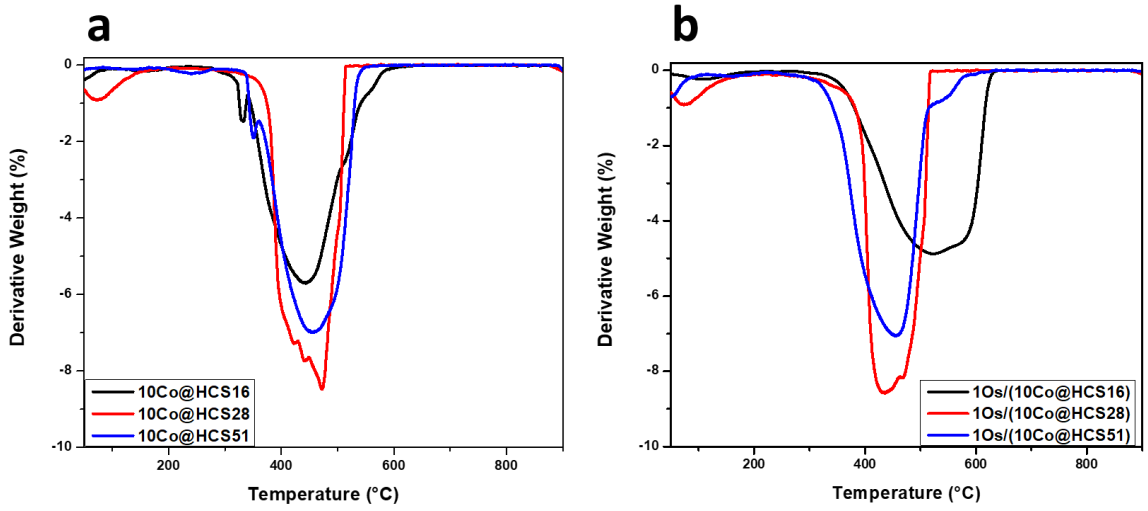

Figure S1: TGA derivative profiles of (a) Co@HCSx and (b) Os/(Co@HCSx) catalysts.

The TGA profiles show that the PSS template was completely removed from the RF shell core during the carbonization procedure and ~10% CoOx metal loading was the remaining residue left after thermal decomposition. This observation emphasizes the efficacy of template removal by thermal decomposition during the CVD process as well as the quality of the synthesized carbon shell. The efficacy of template removal by thermal decomposition is also supported by TEM and XRD studies.

The first derivative profile for Co@HCSx catalysts shown in Fig S1 (a) and (b) occurred between 400 and 500 ℃ thus showing that the HCS was thermally stable. The Co@HCSx catalysts showed a decomposition temperature which agreed with other studies [51, 52]. Furthermore, the Os/(Co@HCS28) and Os/(Co@HCS51) catalysts decomposed at temperatures in the range of 400–500 ℃ while that of the Os/(Co@HCS16) catalyst decomposed above 500 ℃. This was not expected as the carbon shell is thinner in Os/(Co@HCS16) and must relate to the enhanced oxidation of the Co that led to a poorer catalyst to assist any carbon oxidation. The data obtained suggests that the presence of Os on the outer shell did not impact the thermal decomposition of these catalysts as the data were similar to those of the unpromoted Co@HCSx catalysts. Overall, from the TGA profiles it can be deduced that the prepared catalysts were thermally stable for use under FTS reaction conditions.

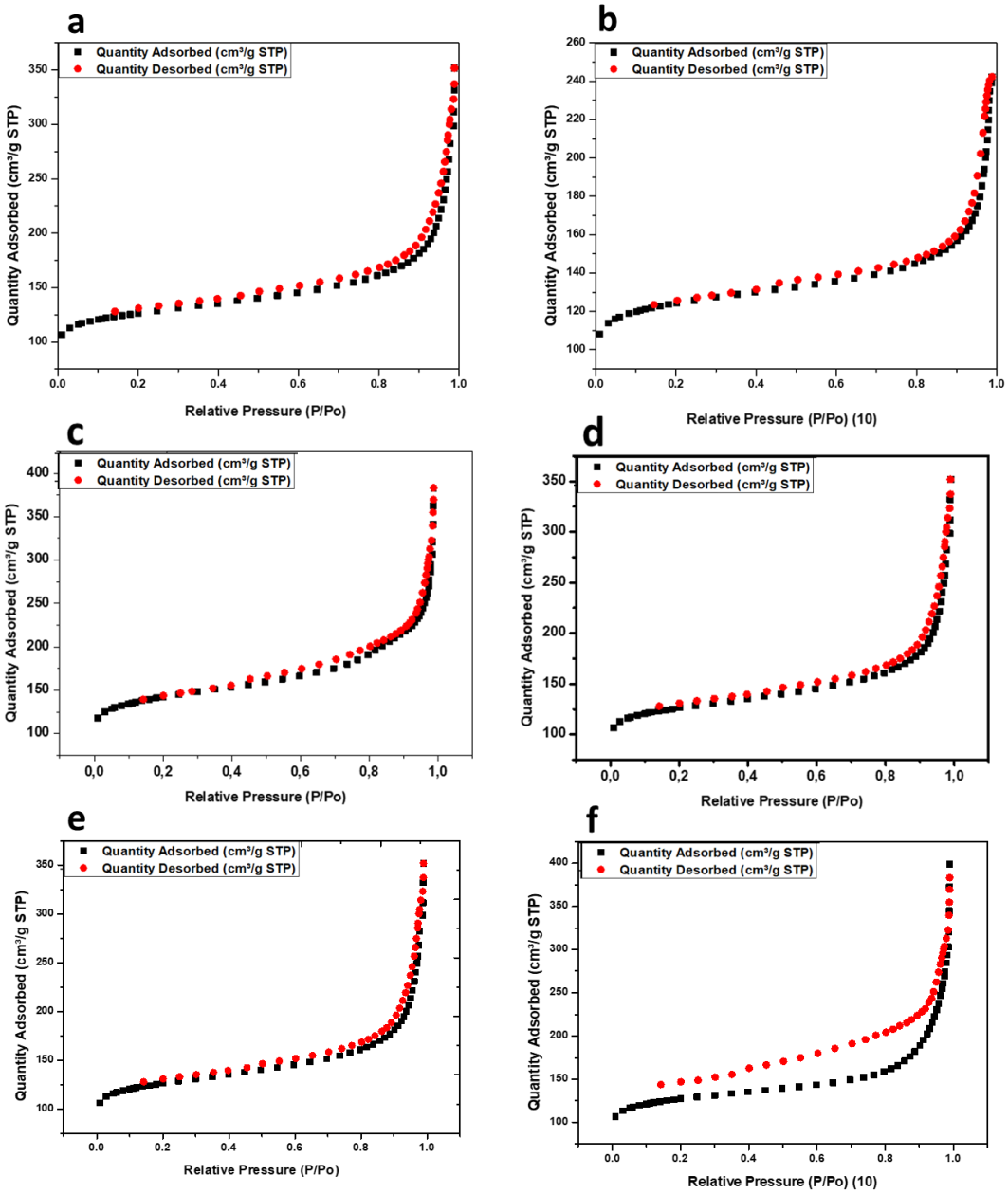

Figure S2: N2 absorption-desorption isotherm curves of the a) 10%C0@HCS16nm, b) 10%Co@HCS28nm,c) 10%C0@HCS51nm, d) 1%Os/10%Co@HCS16nm, e) 1%Os/10%Co@HCS28nm and 1%Os/10%Co@HCS51nm catalysts.

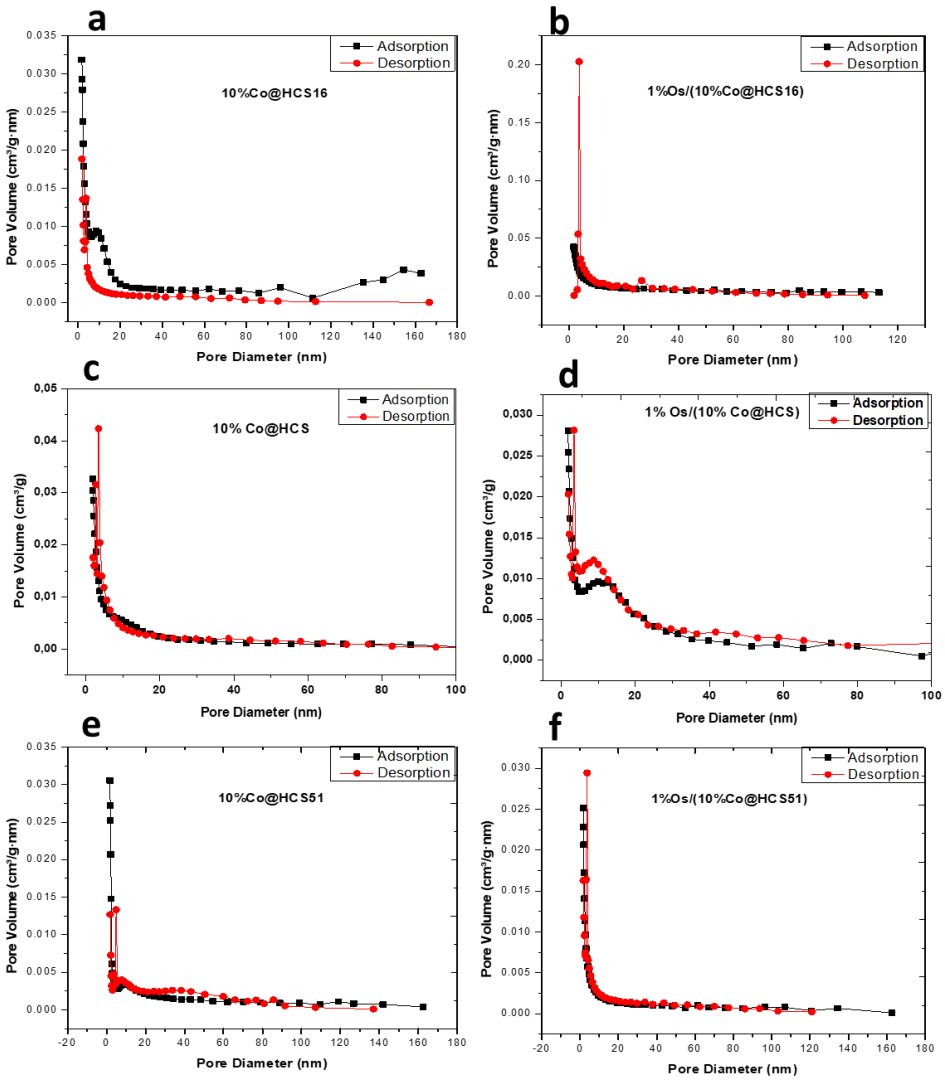

Figure S3: Pore size distribution a) 10%C0@HCS16nm, b) 10%Co@HCS28nm,c) 10%C0@HCS51nm, d) 1%Os/10%Co@HCS16nm, e) 1%Os/10%Co@HCS28nm and 1%Os/10%Co@HCS51nm catalysts.

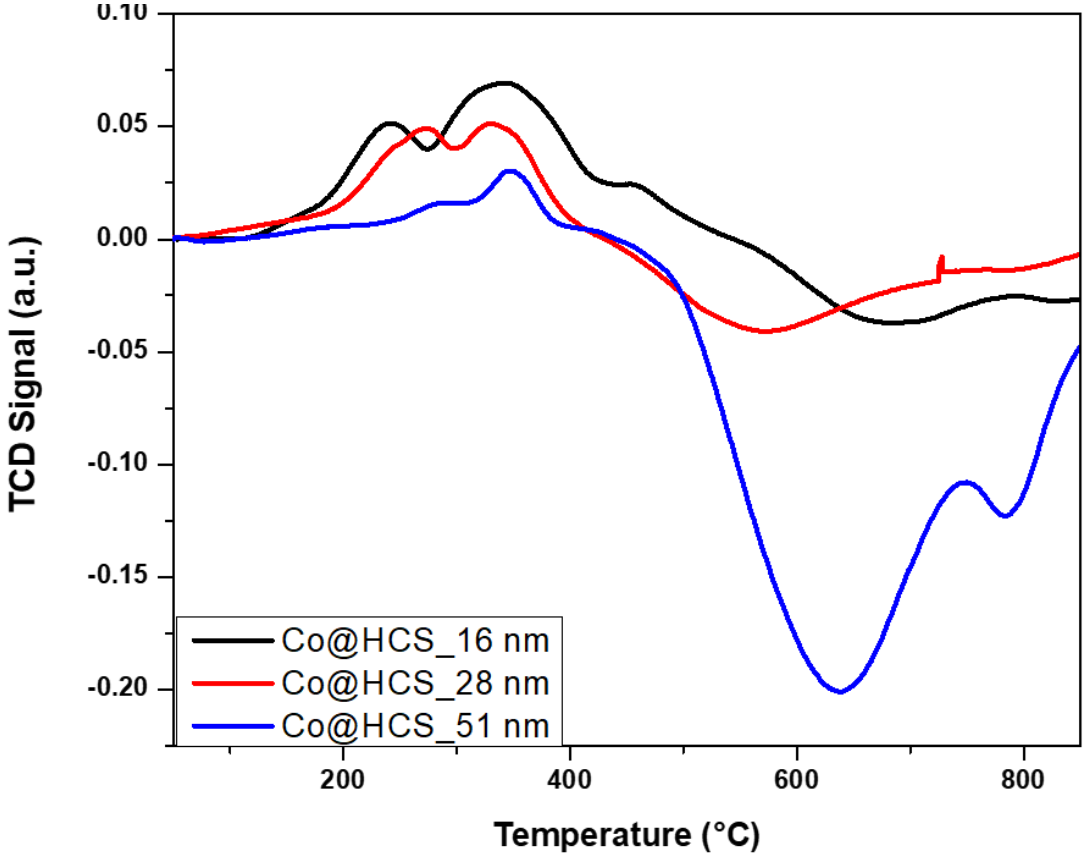

Figure S4: TPR profiles of Co@HCS16, Co@HCS28 and Co@HCS51

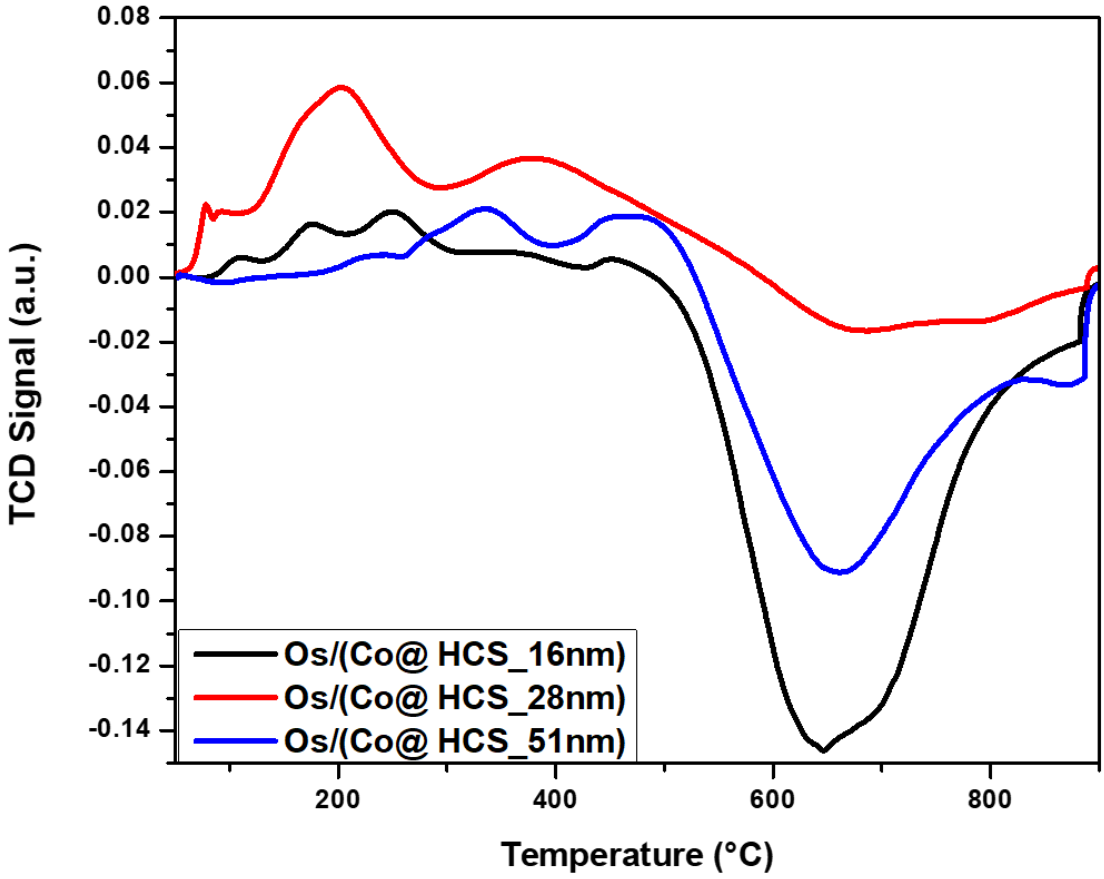

Figure S5: TPR profiles of Os/(Co@HCS16), Os/(Co@HCS28) and Os/(Co@HCS51)

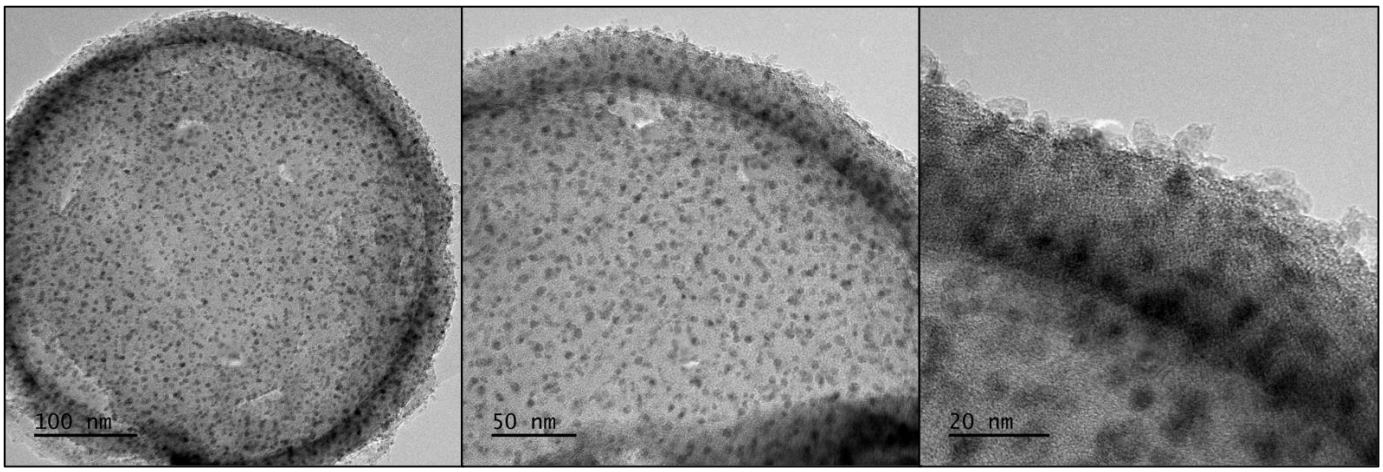

Figure S6: HR-TEM images of Os/10%Co@HCS28 at different magnifications (Scale bar: 100 nm/50 nm/20 nm)

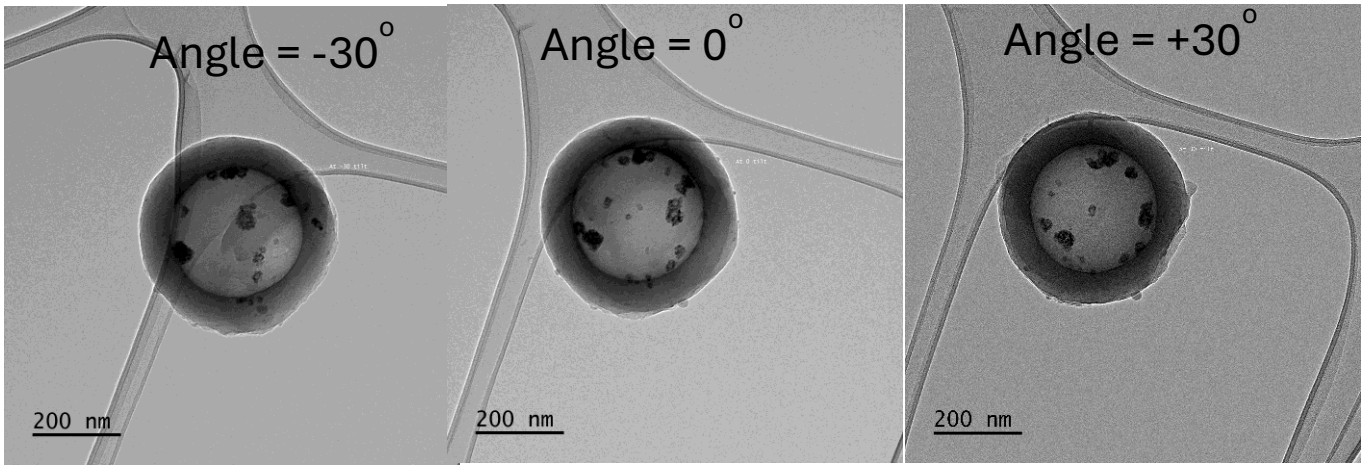

Fig S7(a)

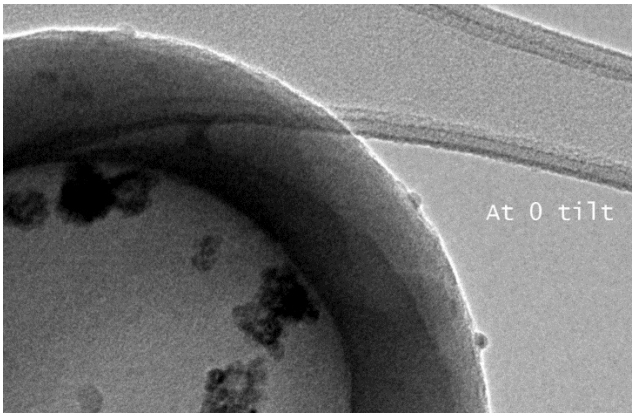

Fig S7(b)

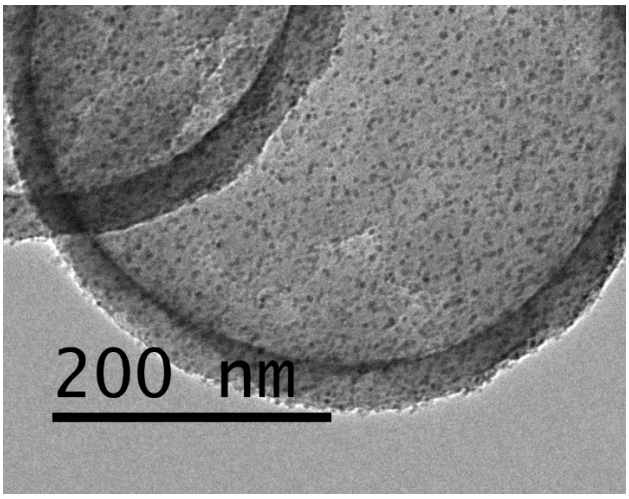

Fig S7(c)

Figure S7: (a)TEM images showing tilting from – 30º to +30º of the 1%Os/Co@HCS51 catalyst. The Figure indicates how the Co particles move within the sphere. (Note that the agglomerated images shown here were recorded on post FT products to show that Co was present in these samples as tilting experiments were not possible with the small catalyst particles used in our study. The TEM image of the freshly made 1%Os/Co@HCS51 is seen in Fig 5 of the paper). Higher magnification TEM images of the sphere surface showing surface metal particles for **(b)** 1%Os/Co@HCS51 and **(c)** 1%Os/Co@HCS28

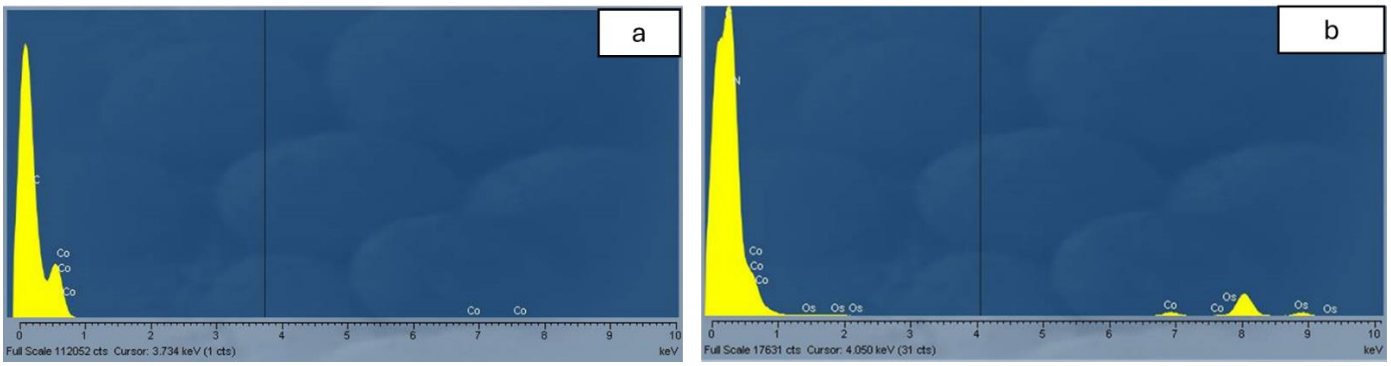

Figure S8: EDX spectrum of (a) Co@HCS and (b) Os/(Co@HCS) catalysts.

The EDX spectra confirmed that both Co and Os nanoparticles were indeed present in both the OsCo@HCS and Os/(Co@HCS) catalysts.

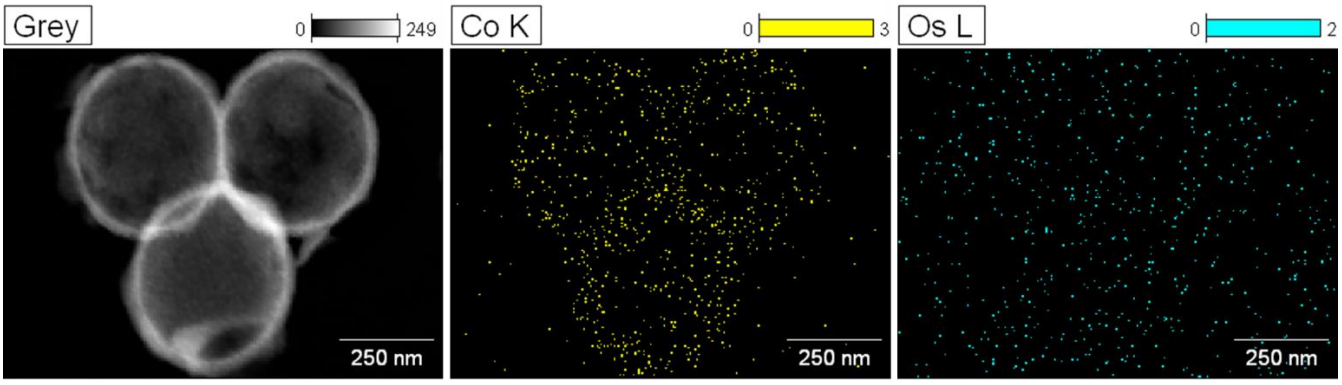

Figure S9: Elemental mapping of 1%Os/(Co@HCS) catalyst

List of Tables

Table S1: Fischer-Tropsch catalytic performance and selectivity (250 °C).

Sample Name	CO conversion (%)	Selectivity (C mol) (%)		
		C_1	C_2-C_4	C_{5+}
10%Co@HCS28	9.8	20.5	13.2	66.3
1%Os/(10%Co@HCS_16 nm)	18.0	16.6	5.8	77.6
1%Os/(10%Co@HCS_ 28 nm)	9.5	17.7	4.4	77.8
1%Os/(10%Co@HCS_51 nm)	2.8	8.2	4.2	87.5